Separation and Purification Technology 149 (2015) 55–64

Contents lists available at ScienceDirect

Separation and Purification Technology

journal homepage: www.elsevier.com/locate/seppur

Photodegradation of 2-chlorophenol over colloidal α-FeOOH supported mesostructured silica nanoparticles: Influence of a pore expander and reaction optimization

R. Jusoh [a], A.A. Jalil [a,b,*], S. Triwahyono [c,d], A. Idris [a], M.Y. Noordin [e]

[a] Department of Chemical Engineering, Faculty of Chemical Engineering, Universiti Teknologi Malaysia, 81310 UTM Johor Bahru, Johor, Malaysia
[b] Centre of Hydrogen Energy, Institute of Future Energy, Universiti Teknologi Malaysia, 81310 UTM Johor Bahru, Johor, Malaysia
[c] Department of Chemistry, Faculty of Science, Universiti Teknologi Malaysia, 81310 UTM Johor Bahru, Johor, Malaysia
[d] Ibnu Sina Institute for Fundamental Science Studies, Universiti Teknologi Malaysia, 81310 UTM Johor Bahru, Johor, Malaysia
[e] Department of Manufacturing and Industrial Engineering, Faculty of Mechanical Engineering, Universiti Teknologi Malaysia, 81310 UTM Johor Bahru, Johor, Malaysia

ARTICLE INFO

Article history:
Received 2 November 2014
Received in revised form 26 April 2015
Accepted 16 May 2015
Available online 23 May 2015

Keywords:
α-FeOOH nanoparticles
Mesostructured silica
Ionic surfactant
Photo-Fenton-like
2-Chlorophenol

ABSTRACTT

In this work, mesostructured silica nanoparticles (MSN) were modified by the pore expander 3-aminopropyl triethoxysilane (APTES) via the sol–gel method before impregnation with a colloidal α-FeOOH-ionic surfactant (IS-FeOOH) to produce IS-FeOOH/MSN_{APTES}. Its properties were characterized using X-ray diffraction, Fourier-transform infrared and surface area analysis, and compared with pristine MSN, MSN_{APTES} and IS-FeOOH/MSNs. The results suggest that IS-FeOOH was located on the outer surface of MSN but in the pores when loaded onto MSN_{APTES}, while retaining its colloidal structure on both supports. It was found that the photoactivity of the catalysts toward photo-Fenton-like degradation of 2-chlorophenol (2-CP) under visible light irradiation was in the following order: IS-FeOOH/MSN (92.2%) > IS-FeOOH/MSN_{APTES} (77.6%) > MSN_{APTES} (38.7%) > MSN (17.5%). The results indicate that the presence of colloidal IS-FeOOH on the outer surface of MSN plays important role in enhancing photoactivity. Photokinetic analysis also supported this result by showing that the surface and bulk reaction was the rate-limiting step for IS-FeOOH/MSN and IS-FeOOH/MSN_{APTES}, respectively. The operating conditions of 2-CP degradation over IS-FeOOH/MSN were further optimized using response surface methodology. The optimum conditions were found to be 9.09 wt% of IS-FeOOH loading with 0.14 mM H_2O_2 at pH 5.11 and 49.9 °C to give 99.9% of the predicted value of photodegradation.

1. Introduction

2-Chlorophenol (2-CP) is an extremely hazardous compound, which is widely used in various chemical processes such as agriculture, paper, cosmetic, biocides, and the public health industry [1]. It presents serious threats to the surrounding ecosystem since chlorinated compounds are also known to be the starting material for dioxins and furans [2]. Thus, efficient treatment is required to avoid the environmental impact caused by this harmful and recalcitrant pollutant. The integration of two different Advanced Oxidation Technologies (AOTs) (photocatalytic and Fenton-like) offers synergistic reaction routes, which have been shown to be suitable for the degradation of various chlorinated phenol pollutants [3–5]. These systems are based on the generation of hydroxyl radicals (·OH), a reactive species, which can react with organic compounds adsorbed onto the photocatalyst surface [6]. Nevertheless, besides enhancing the photoactivity, the adsorption of organic compounds onto the catalyst surface may also cause deactivation to the photocatalyst [7]. Therefore, studying the importance of adsorption in the photocatalytic reaction is very crucial.

α-FeOOH has been widely used as a semiconductor catalyst for the degradation of many chlorinated compounds owing to its unique electrical, optical, and photoluminescent properties [8]. However, α-FeOOH nanoparticles have small surface areas that cause poor photocatalytic performance due to insufficient contact with the reactants [9]. In order to improve the contact between pollutant molecules and the catalyst, the incorporation of a metal oxide onto a mesoporous material support seems to be the most promising method, which has been discussed by several research groups in recent years [10–12]. For instance, mesostructured silica

* Corresponding author at: Department of Chemical Engineering, Faculty of Chemical Engineering, Universiti Teknologi Malaysia, 81310 UTM Johor Bahru, Johor, Malaysia.
E-mail address: aishah@cheme.utm.my (A.A. Jalil).

http://dx.doi.org/10.1016/j.seppur.2015.05.017
1383-5866/

Table 1
Variables showing operating conditions used in central composite design.

Variables	Operating conditions	− Values	+ Values
A	Metal loading (wt%)	5	15
B	pH	3	7
C	H_2O_2 concentration (mM)	0.1	0.2
D	Temperature (°C)	30	50

nanoparticles (MSN) are popular and have been considered excellent potential solid supports for heterogeneous catalysts, due to its distinctive properties such as an ordered porous structure, high surface area (>1000 $m^2\ g^{-1}$), large pore volume, and tunable pore size (1.5–10 nm) [13].

Recently, we have reported on the simple electrosynthesis of colloidal α-FeOOH particles in an ionic surfactant (IS), which inhibited electron-hole recombination and enhanced the photodegradation of 2-CP [14]. It is hypothesized that the incorporation of these colloidal particles onto a mesostructured silica support may improve contact between pollutant molecules and the catalyst and hence enhance the photoactivity. However, it has been reported that it is difficult to control the distribution of active colloidal metal particles over a support [15]. In addition, the supported colloidal metal particles are commonly applied in gas-phase reactions [15] but reports on liquid-phase applications are still rare. Thus, expecting the advantages of the silica support, herein we attempted to support IS-FeOOH on MSN and study its photoactivity toward the degradation of 2-CP. A pore expander, 3-aminopropyl triethoxysilane (APTES), was used to show the discrepancy in the pore size of MSN before loading the electrosynthesized colloidal metal particles. The physicochemical properties of IS-FeOOH/MSN were studied by XRD, FTIR and surface area analysis to clarify its structure. Remarkably, we found that the pore size played an important role in directing the location of the colloidal metal particles on the support, which then affected the photoactivity of the catalysts. A photokinetic analysis was also performed to confirm this result. Then, the operating conditions of the photodegradation using the best catalyst were further optimized using response surface methodology (RSM). It is believed that these findings will lead to extensive studies of using supported colloidal metal particles that are useful for various applications.

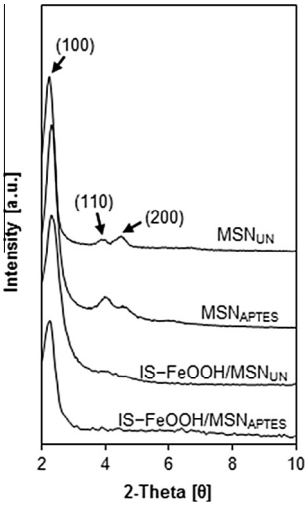

Fig. 1. XRD patterns of catalysts at region 2–10°.

2. Materials and methods

2.1. Materials

2-CP Alfa Aesar® (99% purity) was used without further purification. Mono-cationic IS dodecyltrimethylammonium bromide was purchased from Fisher Scientific, Malaysia. Iron and platinum plates (>99.99% purity) were obtained from Nilaco, Japan. CH_3OH, NaOH and HCl were obtained from HmbG Chemicals, Malaysia. Cetyltrimethylammonium bromide (CTAB), ethylene glycol (EG), and tetraethyl orthosilicate (TEOS) were purchased from Merck, Malaysia. Ammonium hydroxide solution (NH_4OH) was obtained from QRec, Malaysia. Deionized water supplied by the Bibby Sterilin Ltd., UK water treatment system was used to prepare all the solutions.

2.2. Catalyst preparation

MSN were prepared by sol–gel method [16]. The CTAB, EG, and NH_4OH solution were dissolved in 700 mL water with following mole composition, respectively: 0.0032:0.2:0.2:0.1. After 30 min vigorous stirring with heating, 1.2 mmol TEOS were added to give a white suspension solution. This solution was stirred for another 2 h, followed by centrifugation, drying at 333 K and calcined at 823 K for 3 h to give MSN_{UN}. Modification of MSN_{UN} was done by similar procedure but including the 1 mmol APTES addition during the stirring process and then denoted as MSN_{APTES}.

The synthesis procedure of IS-FeOOH nanoparticles were similar to those reported in literature [14,17,18]. 15 mL IS/water solution, with IS to water of 1:1 volume ratio was added to one-compartment cell equipped with magnetic stirring bar and a two-electrode configuration of an iron plate (2 cm × 2 cm) anode and a platinum plate (2 cm × 2 cm) cathode. Electrolysis was conducted at a constant current of 60 mA/cm^2 and 273 K under air atmosphere. The weight percentage of IS-FeOOH supported on MSN was calculated by the time of electrolysis, which is based on the Faraday's law (Eq. (1)),

$$t = \left(\frac{F}{I}\right)(z \times n) \tag{1}$$

where t is the total time for the constant current applied (s); F is the 96,486 C mol^{-1}, which is the Faraday constant; I is the electric current applied (mA); z is the valency number of ions of substance (electrons transferred per ion); and n is the number of moles of substance (number of moles, liberated n = m/M). After electrolysis of 10wt% of IS-FeOOH, the corresponding mixture was impregnated to MSN_{UN} and MSN_{APTES} at 353 K to give IS-FeOOH/MSN_{UN} and IS-FeOOH/MSN_{APTES}, respectively.

2.3. Characterization

Crystallinity study was recorded on D8 ADVANCE Bruker X-ray diffractometer using Cu Kα radiation at 2θ (2–90°). Joint Committee on Powder Diffraction Standards (JCPDS) files was used to identify the phases. The functional groups of IS-FeOOH/MSN were identified using an Agilent Cary 640 Fourier-transform infrared (FT-IR) Spectrometer using the KBr method with a scan range of 400–4000 cm^{-1}. Surface area of IS-FeOOH/MSN was calculated with Brunnauer–Emmett–Teller (BET) method using a Micromeritics ASAP 2010 instrument. The analysis regarding the optical absorption properties of the catalysts were obtained using a PerkinElmer UV–Vis/DRS (Spectrophotometer in the range of 200–800 nm at room temperature. The band gap of catalysts was determined from plots of the Kubelka–Munk (K–M) function [$f_{K-M} = (h\nu/\lambda)^{1/2}$] as a function of the energy of the excitation light [hν].

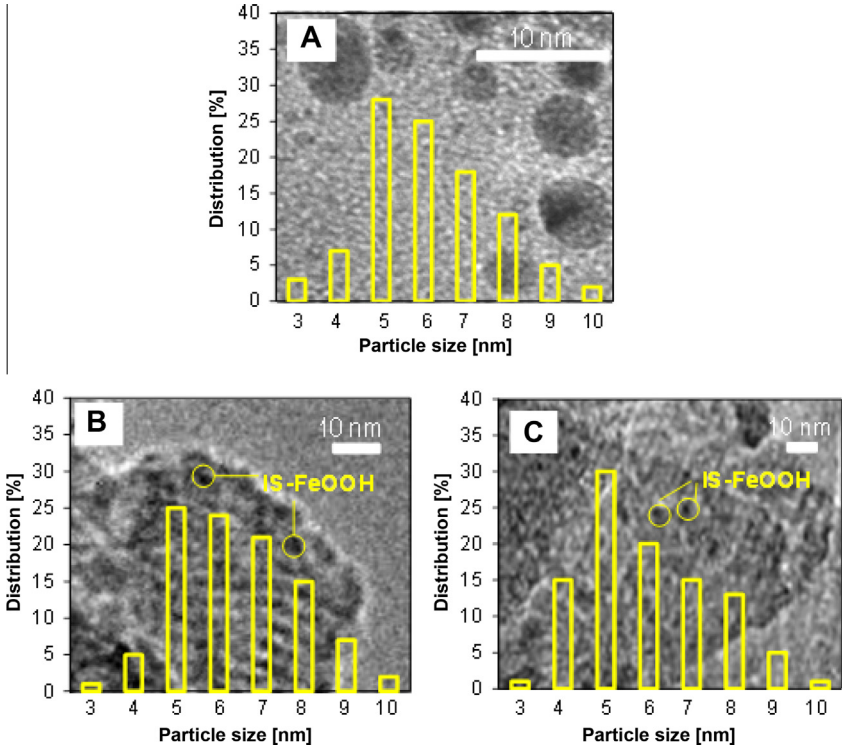

Fig. 2. TEM image and particle size distribution of (A) IS-FeOOH; (B) IS-FeOOH/MSN_{UN}; (C) IS-FeOOH/MSN_{APTES}.

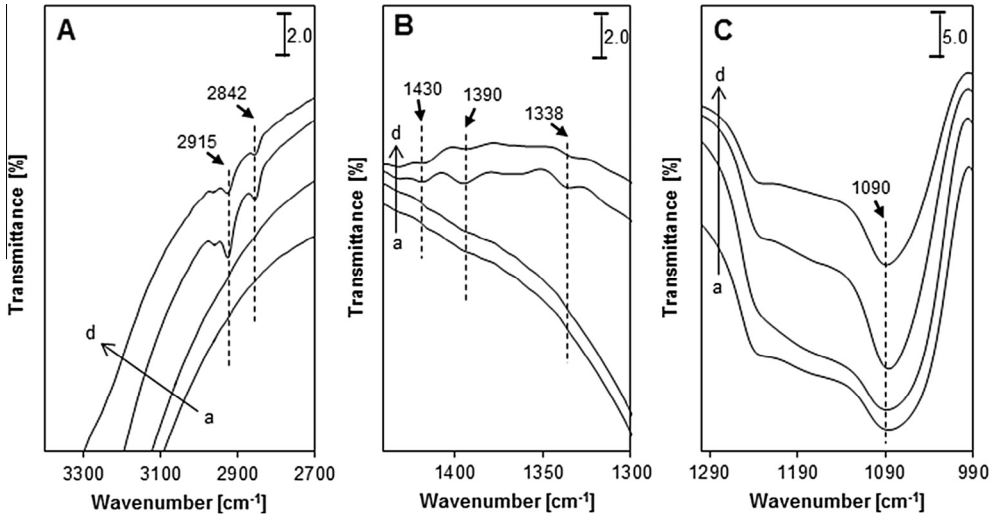

Fig. 3. FT-IR spectra of catalysts. (a) MSN_{UN}; (b) MSN_{APTES}; (c) IS-FeOOH/MSN_{UN}; (d) IS-FeOOH/MSN_{APTES}.

2.4. Catalytic testing

Catalytic activity was tested on a photo-Fenton-like degradation of 2-CP. Catalyst (0.400 g L^{-1}) was added to 50 mg L^{-1} 2-CP solution in a Pyrex batch photoreactor, 140 mm length and 85 mm diameter with a total volume of 0.25 m^3 and was stirred for 2 h in the dark to achieve adsorption–desorption equilibrium with a stirring rate of 250 rpm. Philips TL 20W/52 fluorescent lamp within quartz glass housing (emission spectrum 350–600 nm) with a peak emission at 430 nm was employed as the light source. A quantum sensor connected to a Light Scout quantum light meter indicates the fluorescent light intensity of 50 μmol photons m^{-2} s^{-1}. The entire set-up was placed inside a chamber covered with aluminum foil to prevent the passage of other lights. Initial pH of the solution was 5 and the reaction was carried out at 303 K. Then 0.156 mM hydrogen peroxide (H_2O_2) was added and ambient air was bubbled into the system continuously using an air pump (AC 100–240 V, 12 W motor) before the reaction was performed for another 8 h under visible light irradiation. During the reaction, aliquots of 2 mL were taken out at 15 min intervals and centrifuged in a Hettich Zentrifugen Micro 120 at 75,000 rpm for 10 min before analysis by a double-beam UV–Vis spectrophotometer (Cary 60 UV–Vis Agilent) at 274 nm.

2.5. Experimental design and optimization

A total of four independent variables, $k = 4$ which are metal loading (A), pH (B), H_2O_2 concentration (C), and temperature (D) were selected for the study, where each variable was represented at two levels, high (+) and low (−), as shown in Table 1. The 2-CP

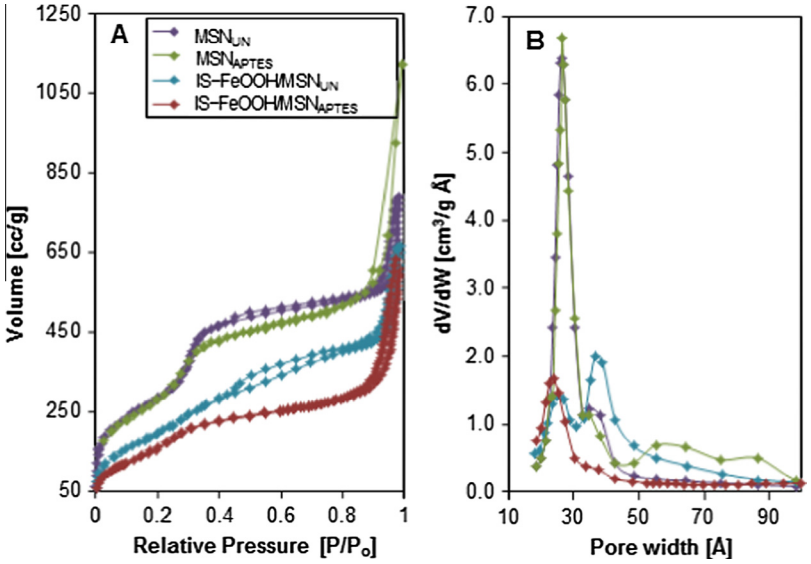

Fig. 4. (A) N_2 adsorption–desorption isotherm; (B) pore size distributions of the catalysts.

degradation percentage (%) was taken as response parameters. The effect of each variable, sum of squares, mean square, *F*-value, *P*-value and confidence level (%) were determined using the statistical software package Design-Expert (Version 7.0.3, State-Ease, Minneapolis, USA).

The full-factorial central composite design consists of a complete $2k$ factorial design, where k is the number of test variables; n_0 centre points ($n_0 \geqslant 1$) and two axial points on the axis of each design variable at a distance of ($=2^{k/4}$, =2 for $k = 4$) from the design centre [19]. Hence, the total number of design points is $N = 2^k + 2k + n_0$. A full−factorial central composite design is used to acquire data to fit an empirical second-order polynomial model [20]. The actual values for the variables at various levels are given in Table S1.

3. Results and discussion

3.1. Characterization

3.1.1. Crystallinity, phase, and structural studies

Fig. 1 shows the small-angle XRD patterns for the MSN, MSN$_{APTES}$, IS-FeOOH/MSN and IS-FeOOH/MSN$_{APTES}$. The patterns show three peaks, indexed as (100), (110), and (200), which are reflections of the typical hexagonally ordered mesostructured silica, demonstrating a high quality of mesopore packing [16]. From the intensities of the (100) peak, it was found that MSN$_{APTES}$ had a greater pore order than pristine MSN. This may be due to the MSN modification by APTES which expanded the pore channels of MSN$_{APTES}$. A similar observation was reported by Aziz et al., who studied the difference between MSN and MCM-41 [13]. They found that MSN had a greater pore size than MCM-41 based on the XRD peak at (100). Meanwhile, the introduction of IS-FeOOH into both MSNs retained the hexagonal structure of the MSNs. However, the formation of the (100) peak was slightly inhibited, while the other two peaks were almost eliminated, signifying a slight loss in MSN hexagonal structural ordering [21]. The absence of IS-FeOOH diffraction peaks in IS-FeOOH/MSNs may be due to the diminutive amount of α-FeOOH species, which was beyond the detection limit of XRD. Similar observations were reported by Setiabudi et al. on the loading of platinum and iridium over an HZSM5 support [22].

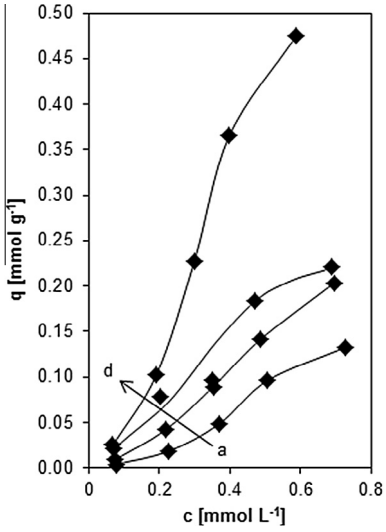

Fig. 5. Adsorption performance of (a) MSN$_{UN}$; (b) IS-FeOOH/MSN$_{APTES}$; (c) IS-FeOOH/MSN$_{UN}$; (d) MSN$_{APTES}$ [pH 5; H_2O_2 concentration is 0.156 mM, catalyst dosage 0.40 g L^{-1}; initial concentration is 50 mg L^{-1}].

3.1.2. Morphological properties

The morphological properties of IS-FeOOH and IS-FeOOH/MSNs were examined by TEM and the results are shown in Fig. 2. Fig. 2A demonstrates the original particles size of IS-FeOOH which mostly in the range of 5–10 nm. It could be observed that the IS-FeOOH are deposited well on the surface of MSN$_{UN}$ (Fig. 2B), while it is located between the lattice fringes when added into MSN$_{APTES}$ (Fig. 2C). This confirmed the role of APTES as a pore expander that allowed the localization of IS-FeOOH in the pore of MSN$_{APTES}$.

3.1.3. Vibrational spectroscopy

All the catalysts were characterized by FTIR spectroscopy to verify bonding between IS-FeOOH and the MSNs (Fig. 3). Two bands were observed at 2915 and 2842 cm^{-1} (Fig. 3A), attributed to the CH_2 stretching vibrations of IS, signifying the existence of IS methylene chains in both the IS-FeOOH/MSN and IS-FeOOH/MSN$_{APTES}$ catalysts [23]. However, the intensity of both bands was lower in the latter than in the former catalyst,

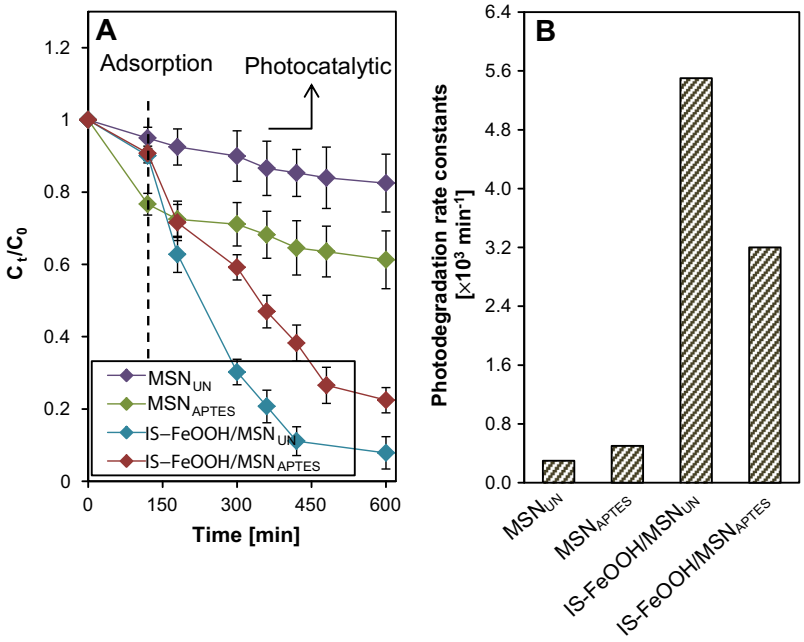

Fig. 6. (A) The 2-CP photodegradation performance; (B) the degradation rate constants of the catalysts [pH 5; H_2O_2 concentration is 0.156 mM, catalyst dosage 0.40 g L^{-1}; initial concentration is 50 mg L^{-1}].

demonstrating that the stretching vibration in IS-FeOOH/MSN_{APTES} is weaker as compared to IS-FeOOH/MSN. The band at 1430 cm^{-1} shown in Fig. 3B for both IS-FeOOH-supported catalysts might correspond to the vibrations of N^+ from the IS head group of IS-FeOOH [14]. The bands observed at 1390 and 1338 cm^{-1} were ascribed to the CH_2 wagging mode of the IS methylene chain [24,25]. The presence of these bands suggests that the colloidal form of IS-FeOOH was retained and well-dispersed on the MSNs. It was recently reported that the IS-FeOOH may physically adsorbed to the MSN surface which induced the attachment of colloidal IS-FeOOH onto the MSN support [28]. Meanwhile, the bands at 1090 cm^{-1} for all catalysts shown in Fig. 3C were attributed to the characteristics of the silica structure, i.e. asymmetric stretching of Si–O–Si bonds [26]. It was observed that the introduction of colloidal IS-FeOOH onto MSNs significantly decreased the band intensity, implying the possible removal of silica by an ion exchange process in the presence of the strong ammonium salt in the colloidal mixture [27]. Furthermore, we have recently reported the possible silica removal from the MSN framework by using a ^{29}Si MAS NMR analysis [28].

3.1.4. Surface area analysis

Nitrogen adsorption–desorption isotherms and the corresponding pore size distribution plots of all catalysts are shown in Fig. 4. All isotherms showed a type IV profile and type H1 hysteresis loops (IUPAC classification), representing the characteristics of mesoporous materials with highly uniform cylindrical pores (Fig. 4A). MSNs samples showed two steps of capillary condensation with the first step at $P/P_o = 0.3$ due to mesopores inside the MSN (intraparticles) and secondly at a higher partial pressure ($P/P_o = 0.9$), which was attributed to interparticle textural porosity. It could be observed that the pristine MSN showed bimodal pore size distributions that consisted of a primary pore at ~2.7 nm and secondary pore at ~3.5 nm (Fig. 4B). The introduction of APTES into MSN maintained both pore distributions and developed larger pores 5.0–9.5 nm in size. When IS-FeOOH was loaded onto pristine MSN, the intrapores decreased significantly while the interpores increased, signifying pore blockage by IS-FeOOH for the former and the possible removal of silica from the MSN framework for the latter case. In contrast, the addition of IS-FeOOH into MSN_{APTES} completely eliminated the pores larger than 3.5 nm. Based on the decrease in Si–O–Si bond intensity in the FTIR results, this confirmed that the additional removal of silica occurred in MSN_{APTES}, thus this most probably allowed the colloidal IS-FeOOH with an original particles size of 5–10 nm [14] to be located in the pore channel. However, due to the smaller pore size in pristine MSN, IS-FeOOH existed only on the surface. The surface area (S_{BET}) of the samples supported this result, in the following order: MSN_{APTES} > MSN > IS-FeOOH/MSN > IS-FeOOH/MSN_{APTES} with values of 1136, 1107, 734, and 529 m^2 g^{-1}, respectively. This result is also in agreement with the XRD data, confirming the reduction of MSN crystallinity upon loading of IS-FeOOH. In addition, this result may also explain the weaker CH_2 stretching vibrations in IS-FeOOH/MSN_{APTES} than in IS-FeOOH/MSN. Remarkably, the results show that pore size modification of the support could control the location of the introduced colloidal IS-FeOOH. Similar variations in catalyst localization have been reported by Lee et al. using different sizes of loaded Pt particles on an SBA-15 support [29].

3.2. Adsorption study

Experimental analysis of the dark adsorption of 2-CP onto the catalysts was performed to study the importance of adsorption for the photo-Fenton-like system; the results are shown in Fig. 5. The capacity of the adsorption, q was found to be in the order MSN < IS-FeOOH/MSN_{APTES} < IS-FeOOH/MSN < MSN_{APTES}. The high adsorption observed for MSN_{APTES} may be due to its high surface area as compared to MSN. Meanwhile, the better adsorption performance of IS-FeOOH/MSNs compared to pristine MSN may due to the existence of the ionic surfactant within the framework and the surface of both IS-FeOOH/MSN_{APTES} and IS-FeOOH/MSN; this would increase the hydrophobicity of the catalysts, which in turn would increase the sorption behavior of the adsorbent toward the adsorption of 2-CP [30]. Based on the Freundlich–type adsorption isotherm, the constant for the degree of nonlinearity between

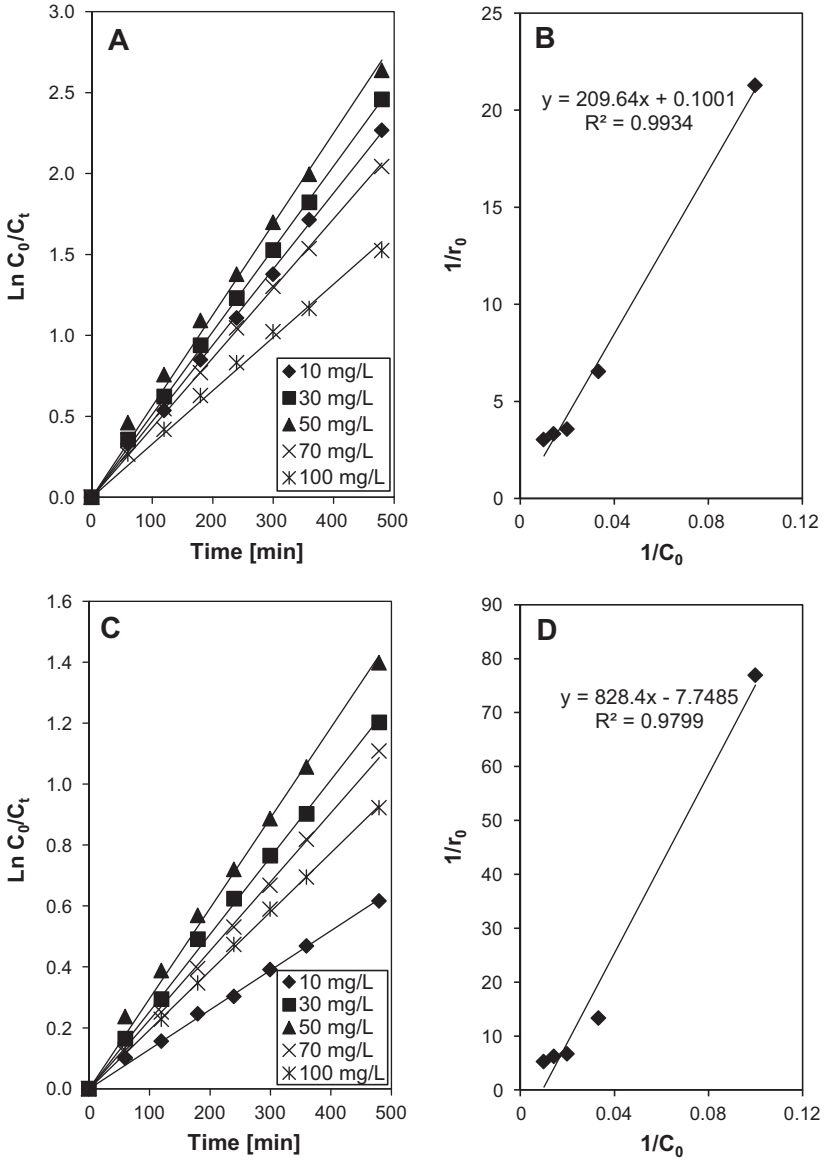

Fig. 7. Photokinetic analysis for (A) and (B) IS-FeOOH/$MSN_{UN;}$ (C) and (D) IS-FeOOH/MSN_{APTES}.

the solution concentration and the adsorption, *n*, was less than 1 for all samples (Table S2). This indicates favorability toward the photo-Fenton-like catalytic system instead of adsorption [31]. Therefore, the photo-Fenton-like reaction was tested to further study the performance of the catalyst.

3.3. Photo-Fenton-like reaction

3.3.1. Performance of the photocatalysts

The performance of all catalysts was examined for the photodegradation of 50 mg L^{-1} 2-CP (Fig. 6A). The degradation activity (C_t/C_0) indicates the adsorption contribution of 0.950, 0.767, 0.901, 0.908 for MSN, MSN_{APTES}, IS-FeOOH/MSN, and IS-FeOOH/MSN_{APTES}, respectively. Subsequently, 17.5% of the 2-CP was degraded under visible light when using the pristine MSN while and MSN_{APTES} gave 38.7% of 2-CP degradation. However, the degradation percentage was increased up to 92.2% when using IS-FeOOH/MSN. The distribution of IS-FeOOH nanoparticles on the surface of MSN might have facilitated their surface contact with light, which led to higher efficiency of degradation [18]. Furthermore, we have recently reported that the retention of IS-FeOOH over MSN support could trap the photogenerated electron while the MSN as a support material could acts as a stable electron acceptor [28]. Meanwhile, a lower degree of degradation of 2-CP was shown by IS-FeOOH/MSN_{APTES} (77.6%), possibly due to the location of colloidal IS-FeOOH in the pores of MSN_{APTES} which hindered visible light accessibility of IS-FeOOH. The band gap energy of the supported catalysts were determined using Kubelka–Munk (K–M) spectrum. The results show lower band gap energy of 3.00 eV when the IS-FeOOH was loaded on MSN_{UN} as compared to the IS-FeOOH/MSN_{APTES} catalyst (3.20 eV). This result is in agreement with the aforementioned results that indicate a higher photodegradation performance by IS-FeOOH/MSN_{UN} catalyst as compared to the IS-FeOOH/MSN_{APTES} catalyst. These may due to the fact that lower band gap energy is generally known to results in efficient performance of photocatalyst.

Fig. 6B shows the photodegradation rate constant of all catalysts. The results reveal that IS-FeOOH/MSN_{UN} gave the highest rate constant of 5.5×10^{-3} min^{-1}, followed by the

Table 2
Analysis of variance (ANOVA) for central composite design for IS-FeOOH/MSN_{UN} catalyst.

Source	Sum of squares	df	Mean square	*F* value	*p*-Value Prob > *F*
Model	6104.280513	14	436.0200366	26.53897534	<0.0001
A	29.57423824	1	29.57423824	1.800077779	0.1891
B	354.7186	1	354.7186	21.59044858	<0.0001
C	0.008261765	1	0.008261765	0.000502864	0.9822
D	4467.566694	1	4467.566694	271.9247566	<0.0001
AB	47.50687813	1	47.50687813	2.891573233	0.0987
AC	24.48250313	1	24.48250313	1.490162131	0.2311
AD	38.65402812	1	38.65402812	2.352732015	0.1349
BC	7.210503125	1	7.210503125	0.438877456	0.5124
BD	118.6185031	1	118.6185031	7.219882724	0.0113
CD	0.219453125	1	0.219453125	0.013357324	0.9087
A^2	0.009982146	1	0.009982146	0.000607577	0.9805
B^2	687.5321298	1	687.5321298	41.84761411	<0.0001
C^2	3.538667861	1	3.538667861	0.215386017	0.6457
D^2	109.4211964	1	109.4211964	6.660075662	0.0147
Residual	525.7415176	32	16.42942243		
Lack of fit	266.2185676	10	26.62185676	2.256759368	0.0536
Pure error	259.52295	22	11.79649773		
Cor total	6811.485381	47			

Table 3
Analysis of variance (ANOVA) for central composite design (reduced) for IS-FeOOH/MSN_{UN} catalyst.

Source	Sum of squares	df	Mean square	*F* value	*p*-Value Prob > *F*
Model	6029.976	7	861.4252	55.98839	<0.0001
A	29.57424	1	29.57424	1.922179	0.1735
B	354.7186	1	354.7186	23.05496	<0.0001
D	4467.567	1	4467.567	290.3698	<0.0001
AB	47.50688	1	47.50688	3.087713	0.0867
BD	118.6185	1	118.6185	7.709617	0.0084
B^2	916.8986	1	916.8986	59.59388	<0.0001
D^2	121.2125	1	121.2125	7.878212	0.0078
Residual	600.0456	39	15.38578		
Lack of fit	340.5226	17	20.03074	1.698025	0.1209
Pure error	259.523	22	11.7965		
Cor total	6811.485	47			

IS-FeOOH/MSN_{APTES}, MSN_{APTES}, and MSN_{UN}, with rate constants of 3.2×10^{-3} min^{-1}, 0.5×10^{-3}, and 0.3×10^{-3} min^{-1}, respectively.

3.4. Photokinetic evaluation

A photokinetic evaluation was performed using the Langmuir–Hinshelwood (L–H) equation in order to further elucidate the photodegradation behavior of the IS-FeOOH/MSN and IS-FeOOH/MSN_{APTES} catalysts (Fig. 7). The simplified L–H equation can be written as a pseudo first-order equation, as in Eq. (2) [18],

$$\ln C_t = -kt + \ln C_0 \tag{2}$$

$$\ln \frac{C_0}{C_t} = kt \tag{3}$$

where C_t is the concentration of 2-CP at time t, C_0 is the initial concentration of 2-CP and k is the reaction rate constant. Eq. (3) represents integrated Eq. (1), where the plot of ln (C_0/C_t) as a function of time was a straight line for both catalysts (Fig. 7A). The results confirm that 2-CP photodegradation catalyzed by IS-FeOOH/MSNs follows first-order kinetics.

The following relationship is obtained when the L–H model is linearized.

$$\frac{1}{r_0} = \left(\frac{1}{k, K_{LH}}\right)\left(\frac{1}{C_0}\right) + \frac{1}{k_r} \tag{4}$$

where k_r is the reaction rate constant and K_{LH} is the adsorption coefficient of the reactant. It was found that for IS-FeOOH/MSN, the calculated k_r and K_{LH} were 9.99 mg L^{-1} min^{-1} and 4.77×10^{-4} L mg^{-1}, respectively. This result illustrates that $k_r > K_{LH}$, suggesting a surface reaction, where 2-CP adsorbed on the catalyst surface is the rate limiting step. This result is in agreement with the adsorption study, which showed the excellent performance of IS-FeOOH/MSN toward the adsorption of 2-CP. Meanwhile, for IS-FeOOH/MSN_{APTES}, the calculated k_r and K_{LH} were -0.13 mg L^{-1} min^{-1} and -9.35×10^{-3} L mg^{-1}, respectively. The result shows that $K_{LH} > k_r$, which indicates that the bulk reaction (photocatalytic reaction with an IS-FeOOH/MSN_{APTES} slurry) is the rate limiting step for the reaction, verifying the hindrance of photocatalytic activity due to the location of colloidal IS-FeOOH in the pores of MSN_{APTES}.

3.5. Process optimization by response surface methodology

Next, an optimization of the photodegradation of 2-CP using the best catalyst, IS-FeOOH/MSN, was carried out by response surface methodology (RSM). In order to ensure a good model, tests for the significance of the regression model and individual model coefficients as well as for lack−of−fit were performed. The summary of the tests is tabulated in an analysis of variance (ANOVA) table shown in Table 2. The value of "Prob. > F" for the model is less than 0.05, indicating that the terms in the model have a significant effect on the response. In the same manner, the main effects of pH (B), reaction temperature (D), the two-level interaction of pH and reaction temperature (BD), and the second-order effect of pH (B^2) and reaction temperature (D^2) were significant model terms.

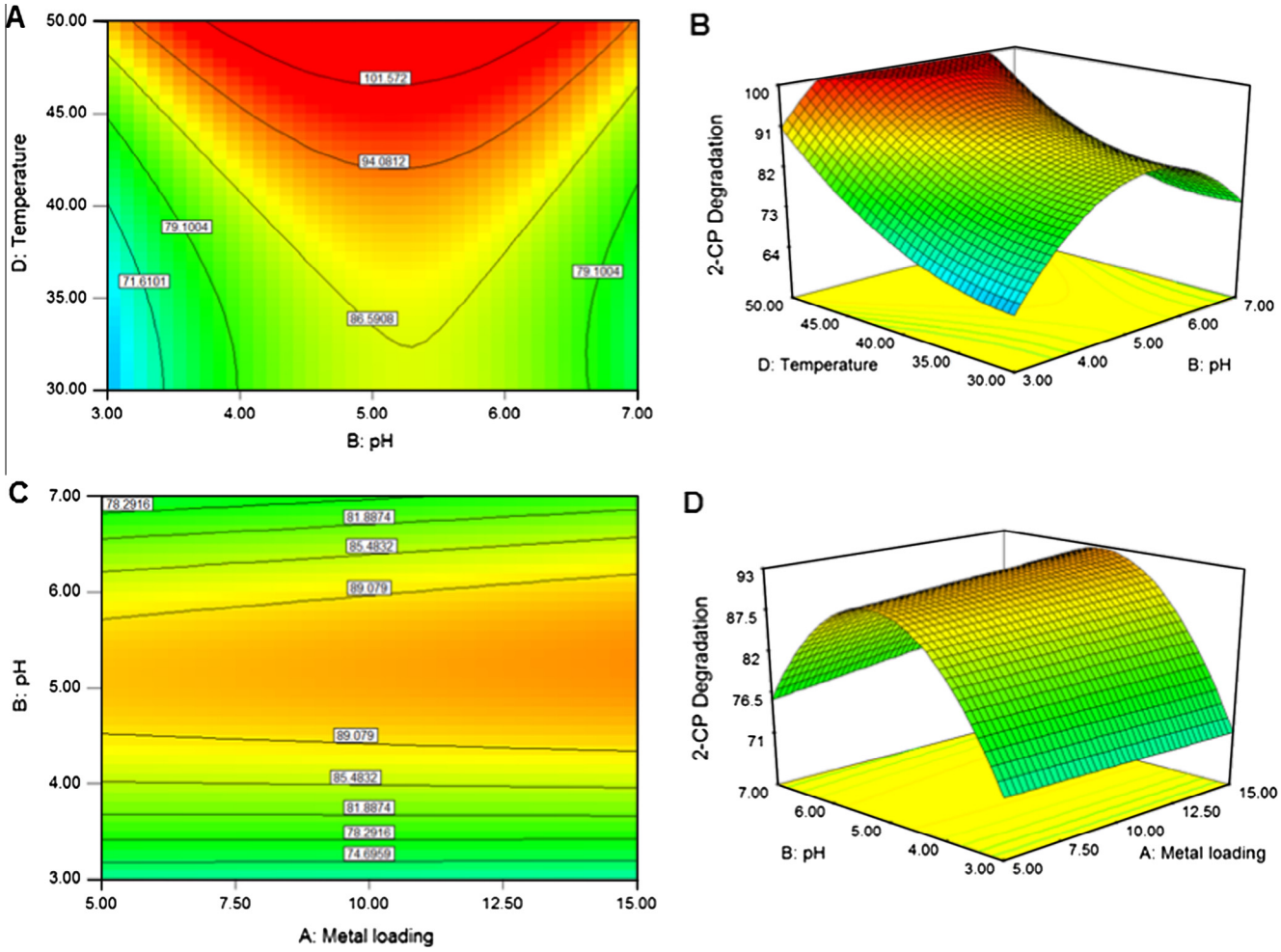

Fig. 8. Contour and response surface plot of (A and B) pH and reaction temperature; and (C and D) IS-FeOOH metal loading and pH.

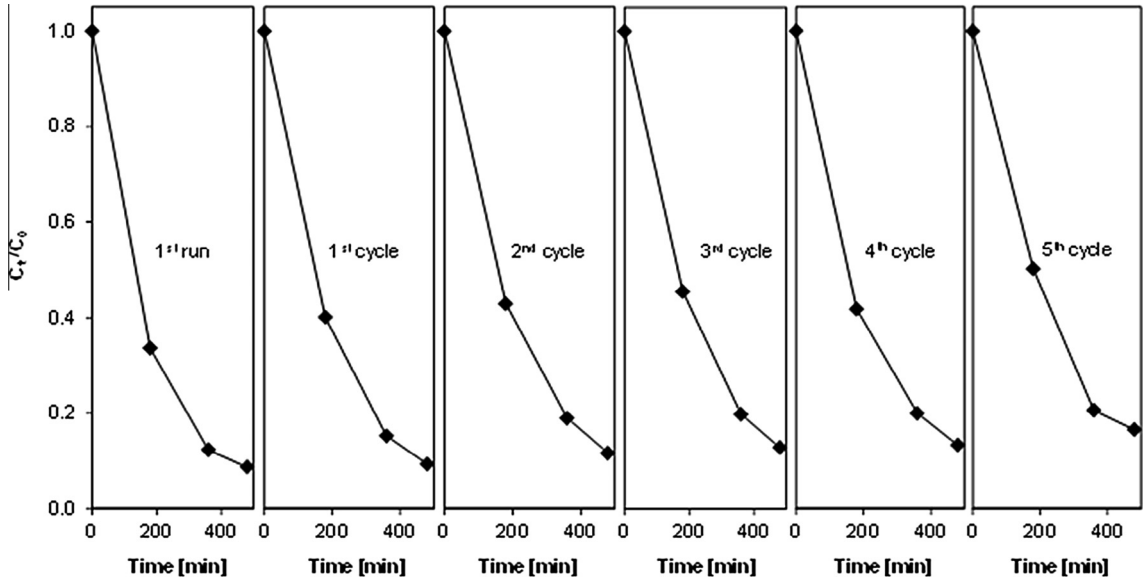

Fig. 9. Stability of IS-FeOOH/MSN_{UN} catalyst after subsequent reactions [pH 5; H_2O_2 concentration is 0.156 mM, catalyst dosage 0.40 g L^{-1}; initial concentration is 50 mg L^{-1}].

The least significant model term, the H_2O_2 concentration (C), was removed to generate an improved model. Additionally, the value of lack–of–fit was found to be insignificant, indicating that desirable fitness of the model was achieved.

Table 3 shows the ANOVA table for the reduced quadratic model of 2-CP degradation by selecting the backward elimination procedure to automatically reduce the terms that are not significant. The results shows that the model is still significant with the main effects of pH (B), reaction temperature (D), the two-level interaction of pH and reaction temperature (BD), and the second-order effect of pH (B^2) and reaction temperature (D^2). The main effect of IS-FeOOH metal loading (A) was additionally added to support the model hierarchy. It was found that both pH (B) and reaction temperature (D) were the most significant factors for the removal of 2-CP.

The R^2 value calculated for the model was 0.909, implying that about 90.9% of the variability in the data is explained by the model [32]. The predicted R^2 was found to be in reasonable agreement with the adjusted R^2, as the adjusted R^2 value is particularly useful when comparing models with different numbers of terms. This comparison is, however, done in the background when model reduction is taking place. Meanwhile, adequate precision compares the range of the predicted values at the design points to the average prediction error. The ratios obtained for this model were greater than 4, indicating adequate model discrimination. The final empirical model in terms of actual factors is depicted in Eq. (5).

$$\begin{aligned}\text{2-CP degradation } (\%) = {} & 15.21759578 - 0.422689338A \\ & + 46.34192434B - 3.270061968D \\ & + 0.12184375AB - 0.096265625BD \\ & - 4.20947368A^2 + 0.061221053D^2 \end{aligned} \quad (5)$$

The normal probability plot of the residuals and the plot of the residuals versus the predicted response for 2-CP degradation are shown in Fig. S1. The plot shown in Fig. S1A reveals that the residuals generally fall on a straight line, implying that the errors are distributed normally; this supports the adequacy of the least-square fit. Fig. S1B indicates no obvious pattern and unusual structure, besides showing equal scatter above and below the x-axis. This implies that the proposed model is adequate and there is no reason to suspect any violation of the independence or constant variance assumption [32].

The contour and three dimensional surface plots demonstrate the effect of different process variables on 2-CP degradation (Fig. 7). The effect of pH (B) and temperature (D), while keeping IS-FeOOH loading (A) at the middle level (10 wt%), is clearly seen in Fig. 8A and B. The degradation of 2-CP increased when the pH changed from 3 to 5.11 and the temperature increased from 30 to 49.94 °C. The maximum 2-CP degradation of 99.99% was observed when the pH was 5.11 and temperature was 49.94 °C. This result could be explained by the decomposition of H_2O_2 at elevated pH. Furthermore, the oxidation potential of $^{\bullet}OH$ was found to be decrease with increasing pH [33]. Meanwhile, a significant enhancement in 2-CP degradation when the temperature was increased may be due to the accelerated rate of oxidizing species generation at higher temperatures [34]. The contour and surface plots of IS-FeOOH metal loading versus pH on the 2-CP degradation are represented in Fig. 8C and D, respectively. It was observed that the pH exhibited a significant influence on 2-CP degradation in comparison with IS-FeOOH metal loading. At constant pH, the effect of IS-FeOOH metal loading on 2-CP degradation was almost negligible, which gave no significant effect on the degradation of 2-CP. Therefore, it appears that pH and the reaction temperature are the dominant factors in 2-CP degradation rather than IS-FeOOH metal loading.

The regression equations obtained using experimental data can be used to predict 2-CP degradation at any particular IS-FeOOH metal loading, pH and reaction temperature within the limits tested. In order to validate the adequacy of the model, four confirmation runs were performed (Table S3). Utilizing the point prediction capability of the software enabled the prediction of 2-CP degradation in the selected experiments within a 95% prediction interval. The predicted values and the actual experimental values were compared and the percentage errors were found to be ~0.6–3.5%. Thus, it can be said that the developed empirical models were reasonably accurate for 2-CP degradation as all actual values for the confirmation runs were within the 95% prediction interval.

3.6. Stability study

Repeated experiments were carried out using IS-FeOOH/MSN in order to study the stability of the catalyst for the degradation of 2-CP (Fig. 9). It can be observed that after four repeated cycles, the catalyst was still active with just a small decrease in 2-CP degradation percentage from 92% to 87%. However, a relatively significant decrease of degradation was observed after the fifth cycle (83%). The results suggest gradual detachment of the colloidal formation on the IS-FeOOH after fifth cycles. In addition, the bonding of the adsorbed pollutant onto the support material may hinder the availability of active sites, which therefore reduced the 2-CP degradation efficiency.

4. Conclusions

In this study, colloidal IS-FeOOH was loaded onto different MSN supports and used in an enhanced photo-Fenton-like degradation of 2-cholorophenol [3,4]. Previous attempts reported MSN with different pore sizes, without further investigation in supported metal use [16]. This study reports pore modification of MSN for the loading of colloidal metal particles, which may provide new insight into the previously reported study on naked nanoparticles loaded onto a mesoporous silica support [35]. It was clearly observed from the FTIR and surface area analysis that the introduction of colloidal IS-FeOOH onto MSN significantly induced silica removal and the immobilization of colloidal IS-FeOOH at different locations on the MSN, depending on the pore size of the MSN. The characterization results also verified the retention of the IS-FeOOH colloidal structure even after being loaded onto MSN.

Photodegradation testing of IS-FeOOH/MSNs showed that the location of colloidal IS-FeOOH on MSN played an important role, depending on the nature of the MSN support. Photokinetic analysis clarified these results by indicating different rate-limiting steps for both IS-FeOOH/MSN catalysts. The reaction conditions of IS-FeOOH/MSN_{UN} were then successfully optimized to provide a new model for the 2-cholorophenol degradation system. Previous reports on supported colloidal metal indicated that the presence of an ionic surfactant in the catalyst system decreased the catalyst activity for the gas-phase reaction [15]. This study, however, indicates that the retention of a colloidal metal over the support material played an important role in enhancing the photocatalytic reaction. Further investigation in this area may contribute to understanding the potential of colloidal metal oxide/mesoporous silica-based solid catalysts for the abatement of organic pollutants on an industrial scale.

Acknowledgements

The authors are grateful for the financial support from Research University Grant Universiti Teknologi Malaysia (Grant No. 4L112), the Exploration Research Grant Scheme from Ministry of Higher Education Malaysia, the awards of the King's Scholarship and Fellowship Scheme from Universiti Malaysia Pahang (Rohayu Jusoh), and the Hitachi Scholarship Foundation.

Appendix A. Supplementary material

Supplementary data associated with this article can be found, in the online version, at http://dx.doi.org/10.1016/j.seppur.2015.05.017.

References

[1] N.C. Tolosa, M.-C. Lu, H.D. Mendoza, A.P. Rollon, The effect of the composition of tri-elemental doping (K, Al, S) on the photocatalytic performance of synthesized TiO_2 nanoparticles in oxidizing 2-chlorophenol over visible light illumination, Appl. Catal. A: Gen. 401 (2011) 233–238.

[2] A.A. Jalil, S. Triwahyono, N.A.M. Razali, N.H.H. Hairom, A. Idris, M.N.M. Muhid, A. Ismail, N.M.N. Yahaya, N.A.L. Ahmad, H. Dzinun, Complete electrochemical dechlorination of chlorobenzenes in the presence of various arene mediators, J. Hazard. Mater. 174 (2010) 581–585.

[3] M. Munoz, Z.M. de Pedro, J.A. Casas, J.J. Rodriguez, Assessment of the generation of chlorinated byproducts upon Fenton-like oxidation of chlorophenols at different conditions, J. Hazard. Mater. 190 (2011) 993–1000.

[4] M. Bertelli, E. Selli, Reaction paths and efficiency of photocatalysis on TiO_2 and of H_2O_2 photolysis in the degradation of 2-chlorophenol, J. Hazard. Mater. 138 (2006) 46–52.

[5] A. Karci, I. Arslan-Alaton, T. Olmez-Hanci, M. Bekbölet, Transformation of 2,4-dichlorophenol by H2O2/UV-C, Fenton and photo−Fenton processes: oxidation products and toxicity evolution, J. Photochem. Photobiol. A 230 (2012) 65–73.

[6] T.E. Agustina, H.M. Ang, V.K. Vareek, A review of synergistic effect of photocatalysis and ozonation on wastewater treatment, J. Photoch. Photobio. C: Rev. 6 (2005) 264–273.

[7] K. Baransi, Y. Dubowski, I. Sabbah, Synergetic effect between photocatalytic degradation and adsorption processes on the removal of phenolic compounds from olive mill wastewater, Water Res. 46 (2012) 789–798.

[8] A. Gajović, A.M.T. Silva, R.A. Segundo, S. Šturm, B. Jančar, M. Čeh, Tailoring the phase composition and morphology of Bi-doped goethite–hematite nanostructures and their catalytic activity in the degradation of an actual pesticide using a photo-Fenton-like process, Appl. Catal. B: Environ. 103 (2011) 351–361.

[9] S. Anandan, A. Vinu, N. Venkatachalam, B. Arabindoo, V. Murugesan, Photocatalytic activity of ZnO impregnated Hβ and mechanical mix of ZnO/Hβ in the degradation of monocrotophos in aqueous solution, J. Mol. Catal. A: Chem. 256 (2006) 312–320.

[10] M.U.A. Prathap, B. Kaur, R. Srivastava, Direct synthesis of metal oxide incorporated mesoporous SBA-15, and their applications in non-enzymatic sensing of glucose, J. Colloid Interface Sci. 381 (2012) 143–151.

[11] K. Niu, D. Shi, W. Dong, M. Chen, Z. Ni, Chelating template-induced encapsulation of NiO cluster in mesoporous silica via anionic surfactant-templated route, J. Colloid Interface Sci. 362 (2011) 74–80.

[12] C. Bouvy, W. Marine, B.-L. Su, ZnO/mesoporous silica nanocomposites prepared by the reverse micelle and the colloidal methods: photoluminescent properties and quantum size effect, Chem. Phys. Lett. 438 (2007) 67–71.

[13] M.A.A. Aziz, A.A. Jalil, S. Triwahyono, R.R. Mukti, Y.H. Taufiq−Yap, M.R. Sazegar, Highly active Ni-promoted mesostructured silica nanoparticles for CO_2 methanation, Appl. Catal. B: Environ. 147 (2014) 359–368.

[14] R. Jusoh, A.A. Jalil, S. Triwahyono, A. Idris, S. Haron, N. Sapawe, N.F. Jaafar, N.W.C. Jusoh, Synthesis of reverse micelle α-FeOOH nanoparticles in ionic liquid as an only electrolyte: inhibition of electron–hole pair recombination for efficient photoactivity, Appl. Catal. A: Gen. 469 (2014) 33–44.

[15] C.-J. Jia, F. Schüth, Colloidal metal nanoparticles as a component of designed catalyst, Phys. Chem. Chem. Phys. 13 (2011) 2457–2487.

[16] A.H. Karim, A.A. Jalil, S. Triwahyono, S.M. Sidik, N.H.N. Kamarudin, R. Jusoh, N.W.C. Jusoh, B.H. Hameed, Amino modified mesostructured silica nanoparticles for efficient adsorption of methylene blue, J. Colloid Interface Sci. 386 (2012) 307–314.

[17] N.W.C. Jusoh, A.A. Jalil, S. Triwahyono, H.D. Setiabudi, N. Sapawe, M.A.H. Satar, A.H. Karim, N.H.N. Kamarudin, R. Jusoh, N.F. Jaafar, N. Salamun, J. Efendi, Sequential desilication–isomorphous substitution route to prepare mesostructured silica nanoparticles loaded with ZnO and their photocatalytic activity, Appl. Catal. A: Gen. 468 (2013) 276–287.

[18] N. Sapawe, A.A. Jalil, S. Triwahyono, S.H. Adam, N.F. Jaafar, M.A.H. Satar, Isomorphous substitution of Zr in the framework of aluminosilicate HY by an electrochemical method: evaluation by methylene blue decolorization, Appl. Catal. B: Environ. 125 (2012) 311–323.

[19] A.I. Khuri, J.A. Cornell, Response Surfaces: Design and Analyses, Dekker, New York, 1987.

[20] R.K. Sen, T. Swaminathan, Response surface modeling and optimization to elucidate and analyze the effects of inoculum age and size on surfactin production, Biochem. Eng. J. 21 (2004) 141–148.

[21] N. Lang, P. Delichere, A. Tuel, Post-synthesis introduction of transition metals in surfactant-containing MCM-41, Microporous Mesoporous Mater. 56 (2002) 203–217.

[22] H.D. Setiabudi, A.A. Jalil, S. Triwahyono, N.H.N. Kamarudin, R.R. Mukti, IR study of iridium bonded to perturbed silanol groups of Pt-HZSM5 for *n*-pentane isomerization, Appl. Catal. A: Gen. 417 (2012) 190–199.

[23] W. Cheng, S. Dong, E. Wang, Synthesis and self-assembly of cetyltrimethylammonium bromide-capped gold nanoparticles, Langmuir 19 (2003) 9434–9439.

[24] N−C. Chia, R. Mendelsohn, Conformational disorder in unsaturated phospholipids by FTIR spectroscopy, BBA-Biomembranes 1283 (1996) 141–150.

[25] M.C. Chang, J. Tanaka, FT-IR study for hydroxyapatite/collagen nanocomposite cross-linked by glutaraldehyde, Biomaterials 23 (2002) 4811–4818.

[26] S. Endud, K.-L Wong, Mesoporous silica MCM-48 molecular sieve modified with $SnCl_2$ in alkaline medium for selective oxidation of alcohol, Microporous Mesoporous Mater. 101 (2007) 256–263.

[27] M. Kerker, Colloid and Interface Science V3: Adsorption, Catalysis, Solid Surfaces, Wetting, Surface Tension, and Water, Academic Press, London, 2012.

[28] R. Jusoh, A.A. Jalil, S. Triwahyono, N.H.N. Kamarudin, Synthesis of dual type Fe species supported mesostructured silica nanoparticles: synergistical effects in photocatalytic activity, RSC Adv. 5 (2015) 9727–9736.

[29] I. Lee, R. Morales, M.A. Albiter, F. Zaera, Synthesis of heterogeneous catalysts with well shaped platinum particles to control reaction selectivity, Proc. Natl. Acad. Sci. USA 105 (2008) 15241–15246.

[30] P.A. Mangrulkar, S.P. Kamble, J. Meshram, S.S. Rayalu, Adsorption of phenol and *o*-chlorophenol by mesoporous MCM-41, J Hazard. Mater. 160 (2008) 414–421.

[31] S.M. Sidik, A.A. Jalil, S. Triwahyono, S.H. Adam, M.A.H. Satar, B.H. Hameed, Modified oil palm leaves adsorbent with enhanced hydrophobicity for crude oil removal, Chem. Eng. J. 203 (2012) 9–18.

[32] A. Idris, F. Kormin, M.Y. Noordin, Application of response surface methodology in describing the performance of thin film composite membrane, Separ. Purif. Technol. 49 (2006) 271–280.

[33] H.R. Eisenhauer, Oxidation of phenolic wastes, J. Water Pollut. Con. F. 36 (1964) 1117–1127.

[34] J-H. Sun, S-P. Sun, G.-L. Wang, L.-P. Qiao, Degradation of azo dye Amido black 10B in aqueous solution by Fenton oxidation process, Dyes Pigm. 74 (2007) 647–652.

[35] T. Suteewong, H. Sai, J. Lee, M. Bradbury, T. Hyeon, S.M. Gruneref, U. Wiesner, Ordered mesoporous silica nanoparticles with and without embedded iron oxide nanoparticles: structure evolution during synthesis, J. Mater. Chem. 20 (2010) 7807–7814.